iJRASET
International Journal For Research in Applied Science and Engineering Technology

INTERNATIONAL JOURNAL FOR RESEARCH

IN APPLIED SCIENCE & ENGINEERING TECHNOLOGY

Volume: 13 **Issue:** VIII **Month of publication:** August 2025

DOI: https://doi.org/10.22214/ijraset.2025.73707

www.ijraset.com

Call: 08813907089 | E-mail ID: ijraset@gmail.com

International Journal for Research in Applied Science & Engineering Technology (IJRASET)
ISSN: 2321-9653; IC Value: 45.98; SJ Impact Factor: 7.538
Volume 13 Issue VIII Aug 2025- Available at www.ijraset.com

Composite Georeferencing Method for Image Processing

Hasan M. Bilani[1], Prof. Ismat M. Elhassan[2], Maan. Okayli[3], Abdullah M. Alanazi[4], Ahmad. Alashaikh[5]
Civil Engineering Department, College of Engineering, King Saud University

Abstract: ***Image georeferencing is the process of accurately mapping an image onto a geographic coordinate system. It is really crucial for applications in remote sensing, urban planning, environmental analysis, and historical research. Numerous studies have evaluated georeferencing methods for their accuracy, efficiency, and application suitability. This paper introduces a new approach, the Composite Georeferencing Method (CGM).***
The CGM begins by applying an Affine or Helmert transformation to align the image control points with their real-world geographic coordinates. Next, a stepwise interpolation process is implemented, utilizing three proposed influence factors: Linear, Cosine, and Tangent. Results indicate that CGM, using these influence factors, yields better outcomes compared to traditional Helmert and Affine methods. Within the first quarter of the maximum distance between points, the Cosine and Tangent Influence Factors show similar performance, while the Linear Influence Factor proves to be less effective. Beyond this point, the Cosine Influence Factor experiences a rapid decline in its effect, which enhances overall performance. In the final quarter of the distance range, the Cosine Influence Factor flattens, becoming negligible, indicating minimal influence of point displacement at longer distances.
Based on these findings, the fifth-degree Cosine Influence Factor is identified as the optimal choice for the Composite Georeferencing Method, offering superior accuracy and efficiency in the georefePrencing process.
Keywords: Transformation, Georeferencing, Interpolation, Image Processing.

I. INTRODUCTION

Image georeferencing can be considered as one of the important pillars for many fields of applied sciences such as remote sensing, environmental analysis, urban planning and archeological research. It has the obvious advantage of improving accuracy and enhancing both comparability, and usability. It, therefore, facilitates the process of decision-making and promotes global collaboration to address environmental, urban, and developmental challenges.

Georeferencing can be defined as the process of assigning real-world geographic coordinates to each pixel of an image, which would allow it to be mapped accurately onto geographic coordinate systems like latitude and longitude. This alignment enables the image to be analyzed in relation to other spatial data, making georeferencing a core function in Geographic Information Systems (GIS) and remote sensing.

Georeferenced aerial photographs play a vital role in ensuring spatial accuracy and integration. They can be overlaid with vector data, such as roads or property boundaries, to create detailed maps used in urban planning and environmental assessments. This integration of data layers is a key factor to simplify both spatial analysis and infrastructure planning.

In remote sensing, georeferencing is essential for integrating satellite imagery with other spatial datasets. Brown and Wilson (2018) have concluded that recent advancements in georeferencing techniques would play an important role in improving the alignment of satellite images with geographic data layers, which leads to enhancing the analysis of environmental changes and land-use patterns.

Georeferenced images are very necessary in urban planning, namely, for studying, monitoring and managing urban sprawl. In their study, Garcia and Martinez (2019) concluded that improved georeferencing techniques provide a means for reaching detailed assessments of urban growth, enforcing better-informed decisions regarding infrastructure, land management, and city development.

Another significant benefit of georeferencing is the consistency and comparability it offers. High temporal resolution georeferenced satellite images allow monitoring land use changes, deforestation and urban growth. On the other hand, high spatial resolution georeferenced satellite images provide accurate spatial data which is vital for natural resource management and urban planning.

Georeferencing is usually performed using specialized GIS software such as ArcGIS, QGIS, and ERDAS IMAGINE. Moreover, quick and obvious progress in machine learning and automated algorithms has also been a major factor to improve the efficiency and accuracy of the georeferencing process, reducing manual intervention and increasing precision.

A. *Techniques in Image Georeferencing*

Image Georeferencing techniques can be classified as either Manual, Automatic or Machine Learning. These can be outlined as follows:

- Manual Georeferencing: This approach is based on manually selecting control points on an image and matching them with their corresponding geographic coordinates. Although this approach is time-consuming, it is however, essential for applications that demand high precision, such as working with historical maps or images with substantial distortions.
- Automatic Georeferencing: This approach is a result of the noticeable and quick development in image processing and computer vision techniques. Automatic Georeferencing techniques utilize algorithms to detect and match features between an image and a reference dataset. By this they significantly reduce the need for manual input. Recent developments have introduced feature-based methods for image georeferencing. As an example, the study by Miller and Zhang (2015) explored the use of feature detection algorithms like SIFT (Scale-Invariant Feature Transform) and SURF (Speeded-Up Robust Features), which automatically identify and match features between images and geographic maps. These techniques would obviously improve georeferencing accuracy by minimizing reliance on manually selected control points.
- Machine Learning Techniques: Machine learning has played a recognizable role in revolutionizing image georeferencing. Li et al. (2020) employed convolutional neural networks (CNNs) to automate the georeferencing process. Their study has achieved impressive accuracy and robustness. Their research underscores the potential of deep learning to handle complex geospatial data and enhance georeferencing performance, even in challenging conditions.

B. *Challenges in the Georeferencing Process*

- Image Distortion: Aerial and satellite images often suffer from distortions caused by sensor orientation, terrain variations, or atmospheric conditions. These distortions affect the alignment of consecutive images with the actual ground coordinates. Hence, correction of these distortions is necessary for accurate georeferencing.
- Control Point Selection: The precision of georeferencing largely depends heavily on the quality accuracy and distribution of control points. If control points are poorly selected or unevenly spaced, it may cause significant errors in the transformation process which can lead to reduction of the overall accuracy.
- Resolution and Scale: The image's resolution and the reference data's scale are highly effective factors in georeferencing. High-resolution images usually require more precise control points to maintain accuracy, while low resolution images are not expected to lead to high accuracy due to insufficient detail, making it difficult to achieve precise georeferencing.

II. LITERATURE REVIEW

Historically, image georeferencing was used to be done through manual methods making use of control points. Researchers such as Smith et al. (1995) explored early affine transformation techniques, manually aligning images with ground control points (GCPs) identified on maps. Although foundational, these methods often faced limitations in terms of accuracy and efficiency. Although these methods are quite basic and recognizable they often faced limitations in terms of accuracy and efficiency.

In the late 1990s, significant advancements were made with the introduction of polynomial transformations. Jones and Brown (1998) demonstrated that polynomial equations are more relevant to model the relationship between image and geographic coordinates compared to simple affine transformations, thus improving accuracy by addressing complex distortions.

Over time, image georeferencing methods progressed from manual techniques to sophisticated algorithms and machine learning approaches. Recent improvements have significantly enhanced both the accuracy and automation of georeferencing, particularly in applications like remote sensing and urban planning. Future research should focus on further automating these processes, integrating diverse data sources, and addressing georeferencing challenges in complex environments.

In the study by Yuan and Elaksher (2007) the methods for georeferencing historical aerial photographs using GIS and image processing techniques have been explored. The study emphasized the importance of accurate control points and suggested solutions to issues such as image distortion. Chiabrando, Donadio, and Rinaudo (2016) investigated the use of machine learning and crowdsourcing to automate the georeferencing of historical maps, demonstrating how these techniques can enhance both accuracy and efficiency.

In their study, Zhang and Luo (2018) addressed real-time image georeferencing using UAVs (Unmanned Aerial Vehicles), proposing methods to integrate real-time georeferencing into UAV-based remote sensing. On the other hand, Li, Wang, and Zhang (2012) focused on georeferencing satellite images using GCPs and feature matching. They also discussed the feasibility of utilizing various interpolation methods and discussed the crucial role of control point selection.

Rumsey and Williams (2002) examined the challenges of georeferencing historical maps in a GIS framework, particularly focusing on how historical map distortions impact the georeferencing process. McDaid and Long (2019) compared georeferencing algorithms for historical maps. They have concluded that machine learning-based methods generally outperformed traditional techniques in both accuracy and efficiency. They also highlighted the critical importance of high-quality control points.

Campbell and Wilke (2020) proved that leveraging OpenStreetMap (OSM) data significantly improves the automation of image georeferencing, reducing the need for manual intervention while increasing accuracy. Johnson and O'Reilly (2021) applied convolutional neural networks (CNNs) for georeferencing remote sensing images, demonstrating superior accuracy and robustness, particularly in challenging environments.

Liu, Zhang, and Chen (2018) introduced a hybrid georeferencing method combining feature-based and pixel-based techniques, striking a balance between precision and computational efficiency, making it ideal for high-resolution satellite imagery. Peters and Smith (2022) reviewed the use of control points in image georeferencing. The emphasized the fact that the quality and distribution of control points are critical to georeferencing accuracy. Moreover, they recommended best practices for optimal results.

Several studies have also compared georeferencing methods to evaluate their accuracy, efficiency, and suitability for various applications. Notable comparisons include:

Martinez and Garcia (2017) carried out a comparison between traditional georeferencing methods including affine and polynomial transformations with modern feature-based techniques such as SIFT and SURF. Their findings showed that feature-based methods provided higher accuracy and better handling of distortions, though polynomial transformations remained effective with high-quality control points.

Smith and Brown (2018) compared various georeferencing techniques, including affine, projective, and machine learning-based methods for remote sensing imagery. They found concluded that machine learning techniques, particularly those using CNNs, outperformed are superior to traditional methods in accuracy and robustness, indicating the potential of machine learning for complex geospatial data.

Johnson and Wang (2019) compared automated georeferencing methods with manual approaches using high-resolution satellite imagery They concluded that automated methods, such as feature-based and machine learning techniques, are more efficient and time-saving, although manual methods offered greater precision in cases with fewer control points.

Liu and Chen (2020) studied the feasibility of using hybrid georeferencing approaches, combining traditional methods with modern techniques. Their study proclaimed that hybrid methods integrating affine transformations with feature-based techniques enhanced accuracy and robustness, offering a versatile solution for various georeferencing challenges.

Lee and Park (2021) compared algorithms utilizing OSM data, including feature matching, control points, and machine learning-based methods. Their research demonstrated that algorithms using OSM data significantly improved georeferencing accuracy and automation, with machine learning methods excelling at aligning images with OSM data.

In general, these studies collectively illustrate clearly the evolution of image georeferencing techniques, highlighting their respective strengths and weaknesses. Advances in machine learning and hybrid approaches have generally improved accuracy and efficiency, though traditional methods continue to be valuable in specific contexts.

III. COMPOSITE GEOREFERENCING METHOD (CGM)

Let's consider a set of *r* points in an image for which the ground coordinates have been measured using GPS. This set is divided into two groups: *n* control points and *m* check points. We will denote the following:

X_i, Y_i are the coordinates of control points (CP)on the ground (*i=1, 2, …..., n*).

Xc_k, Yc_k are the coordinates of check points (Ch.P)on the ground (*k=1, 2, …, m*).

$\hat{X}_i, \hat{Y}_i$ and $\widehat{Xc}_k, \widehat{Yc}_k$ are consequently, the coordinates of the CP and Ch.P within the image.

$\hat{X}_{i0}, \hat{Y}_{i0}$ represent the coordinates of CP after applying the Affine (or Helmert) Transformation.

$\hat{X}_{ji}, \hat{Y}_{ji}$ represent the coordinates of CP after applying the step-wise CGM with respect to point *i.*

$\widehat{XC}_k, \widehat{YC}_k$ represent the coordinates of Ch.P, calculated by the transformation parameters.

$D_{i,j}$ is represents the distance between point i and point *j*.

$$D_{i,j} = \sqrt{(X_i - X_j)^2 + (Y_i - Y_j)^2} \qquad (1)$$

i; j =1, 2, 3, ……..., m+n).

In the first step, we apply the Affine or Helmert transformation using a set of *n* control points, which generates new coordinates $\hat{X}_i, \hat{Y}_i$. However, the image's pixel coordinates may not perfectly align with the geographic coordinates X_i, Y_i measured by GPS. The CGM is then used as an interpolation approach to ensure that each pixel is assigned an accurate location. CGM aims to maintain consistency between the control points and their actual geographic positions, improving overall georeferencing accuracy.

he second step introduces an influence factor, which determines how the displacement of one point affects the surrounding points. This influence factor helps distribute the positional adjustments across the image, ensuring that any correction applied to a control point is smoothly propagated to nearby points, thereby improving the overall spatial accuracy of the georeferencing process.

The concept of the proposed CGM involves stepwise shifting of the control points $\hat{X}_i, \hat{Y}_i$ so that they align with the true coordinates` X_i, Y_i. This process creates mutual influence among the other points, meaning that shifting any point i (where *i = 1, 2, …, n*) will affect the other points j (where *j = 1, 2, …, n-1*). The shift for point j is should be inversely proportional to the distance $D_{i,j}$between points i and j. This effect can be expressed as: $\Delta X = (X_i - \hat{X}_i)\, f(D_{i,j})$ and $\Delta Y = (Y_i - \hat{Y}_i)\, f(D_{i,j})$, where $f(D_{i,j})$ is the influencing factor on point j due to shifting of point i. The function $f(D_{i,j})$ should be designed such that the effect of shifting point i on point j decreases as the distance $D_{i,j}$ between them increases.

Therefore, the second step involves proposing a suitable form for the influence factor $f(D_{i,j})$. Based on the concept that nearby points significantly affect one another during the georeferencing process, the following forms can be suggested:

- The Linear Influence Factor $f(D_{i,j}) = \left[1 - \left(\frac{D_{i,j}}{D_{max}}\right)\right]^r$ (2)
- The Cosine Influence Factor $f(D_{i,j}) = cos^r\left(\frac{D_{i,j}}{D_{max}} \cdot \frac{\pi}{2}\right)$ (3)
- The Tangent Influence Factor $f(D_{i,j}) = tan^r\left[\left(1 - \frac{D_{i,j}}{D_{max}}\right) \cdot \frac{\pi}{4}\right]$ (4)

Where D_{max} is the maximum distance between control points, and *r* is a parameter ($r \geq 1$).

It is clear that, in the above suggested forms there is no influence of point i on point j when they are separated by D_{max}.

The third step in the CGM involves shifting the point $(\hat{X}_i, \hat{Y}_i)$ so that it aligns with its actual coordinates (X_i, Y_i) for each *i=1,2,…,n.* Each adjustment at point i will subsequently influence the coordinates of the other points *j* (*j=1, 2, …,n*), resulting in step-wise updated coordinates for all point.

Beginning with the shift of point *1* (where *i=1*), the updated coordinates for the other points *j* can be expressed as follows:

$$\begin{pmatrix} \hat{X}_{j1} = \hat{X}_{j,0} + (X_1 - \hat{X}_{j,0})\, f(D_{1j}) \\ \hat{Y}_{j1} = \hat{Y}_{j,0} + (Y_1 - \hat{Y}_{j,0})\, f(D_{1j}) \end{pmatrix} \quad (5)$$

Then, shifting of point *2* gives:

$$\begin{pmatrix} \hat{X}_{j2} = \hat{X}_{j,1} + (X_2 - \hat{X}_{j,1})\, f(D_{2j}) \\ \hat{Y}_{j2} = \hat{Y}_{j,1} + (Y_2 - \hat{Y}_{j,1})\, f(D_{2j}) \end{pmatrix} \quad (6)$$

Thus, we can generalize the process so that, at each step *i* (*i = 1, 2, 3, …, n*) of step-wise georeferencing, a shift is applied to point i will result in updated coordinates $(\hat{X}_{j,i}, \hat{Y}_{j,i})$ with respect to those $(\hat{X}_{j,i-1}, \hat{Y}_{j,i-1})$ obtained from the previous shift. This iterative adjustment process can be expressed as:

$$\begin{pmatrix} \hat{X}_{ji} = \hat{X}_{j,i-1} + (X_i - \hat{X}_{j,i-1})\, f(D_{ij}) \\ \hat{Y}_{ji} = \hat{Y}_{j,i-1} + (Y_i - \hat{Y}_{j,i-1})\, f(D_{ij}) \end{pmatrix} \quad (7)$$

i= 1,2 …, n ; j= 1, 2, …, n

This formulation allows for the cumulative refinement of coordinates across all points as each control point is adjusted in a stepwise manner.

As a result, the coordinates $\hat{X}_i, \hat{Y}_i$ obtained from the Affine/Helmert Transformation will be updated after each shift, leading to the final coordinates of the control points $(X_{n,n}, Y_{n,n})$.

Simultaneously, shifts one through *n* influence on the *m* check points, updating their coordinates as follows:

$$\begin{pmatrix} \widehat{Xc}_{ki} = \widehat{Xc}_{k,i-1} + (Xc_k - \widehat{Xc}_{k,i-1})\, f(D_{ik}) \\ \widehat{Yc}_{ki} = \widehat{Yc}_{k,i-1} + (Yc_k - \widehat{Yc}_{k,i-1})\, f(D_{ik}) \end{pmatrix} \quad (8)$$

k= 1,2 ……, m

IV. APPLICATION

We will implement the proposed methodology on a LIDAR image of a region in Cairo City, Egypt as an example. In this image, /12/ distinct points were chosen so that, their coordinates can be measured on the ground using GPS. Table 1 displays the coordinates of these points both in the image and on the ground, while Figure 1 illustrates their distribution.

Table 1 The coordinates of ground control points measured by GPS, along with the corresponding coordinates of these points in the LIDAR image

Point Number	LiDAR Image Coordinates		GCP Coordinates	
	Input E (m)	Input N (m)	Reference E (m)	Reference N (m)
1	640817.488	815658.553	640823.884	815654.260
2	643308.990	814022.489	643319.115	814017.253
3	642160.433	815834.003	642169.052	815827.228
4	643174.952	815712.007	643182.851	815707.218
5	641362.932	814901.340	641373.391	814896.485
6	642155.981	815028.894	642164.775	815020.437
7	640718.069	814243.871	640726.597	814235.5 08
8	641681.992	814390.075	641691.846	814383.120
9	641111.518	813609.341	641117.291	813604.129
10	643243.460	814719.870	643250.951	814715.879
11	641547.972	815285.054	641554.194	815278.540
12	642460.984	814380.024	642469.085	814375.358

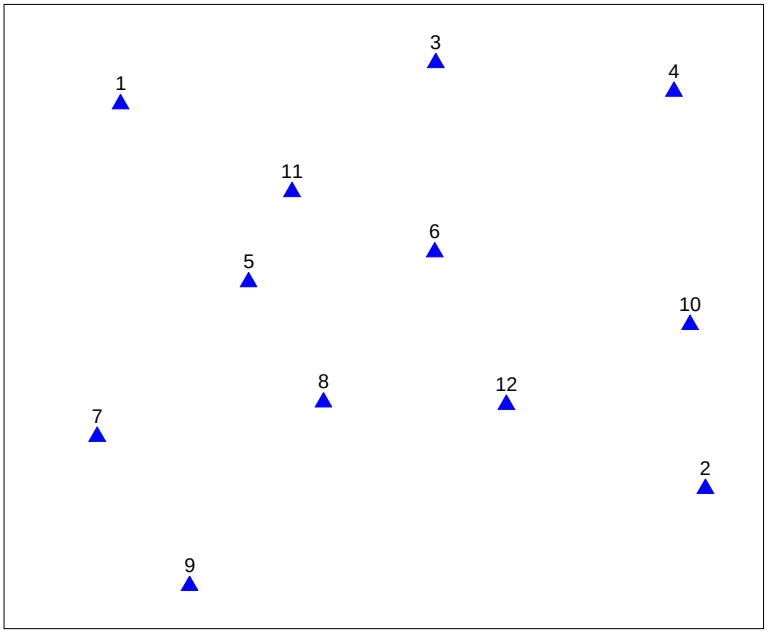

Fig. 1 Distribution of ground control points

Initially, an affine transformation was applied using ten control points, with the remaining two points designated as check points. This step resulted in the preliminary georeferencing of the image, where all control points were closely aligned with their actual positions based on the least squares principle. Displacements between the affine-transformed points and their true positions were then calculated.

In the second phase, the proposed methodology (CGM) was applied to the affine-transformed points. This process involved using different ratios of points for the modeling, alongside various influence factor cases, each characterized by different shapes and internal parameters r. During the modeling, one check point was maintained, and the number of modeling points varied with ratios of 1:5, 1:3, and 1:2.

Experiment 1: The CGM was applied using a linear Influence Factor (*as per equation 2*), with varying values of the internal parameter *r* and different ratios of check points to modeling points: 1:5, 1:3, and 1:2. After recalculating the new coordinates, the displacements of the check points from their actual positions were measured. The maximum, average, and standard deviation of these displacements were determined.

Figure 2 shows the maximum, mean, and standard deviation values of the check point displacements after applying the linear Influence Factor with *r = 1*. The figure reveals that using one check point per three or five control points yields similar results, both outperforming the 1:2 ratio.

When *r* was increased to 2, the results improved compared to *r = 1* (Fig. 3). However, increasing *r* to 3 or 4 did not lead to further improvement beyond *r = 2*, as illustrated in Figures 4 and 5.

The experiment concluded that the second-degree linear Influence factor produced the best results. Figure 6 compares the CGM (using the second-degree linear Influence Factor) with Affine and Helmert transformations, showing that CGM outperformed both methods, as demonstrated in Figure 6.

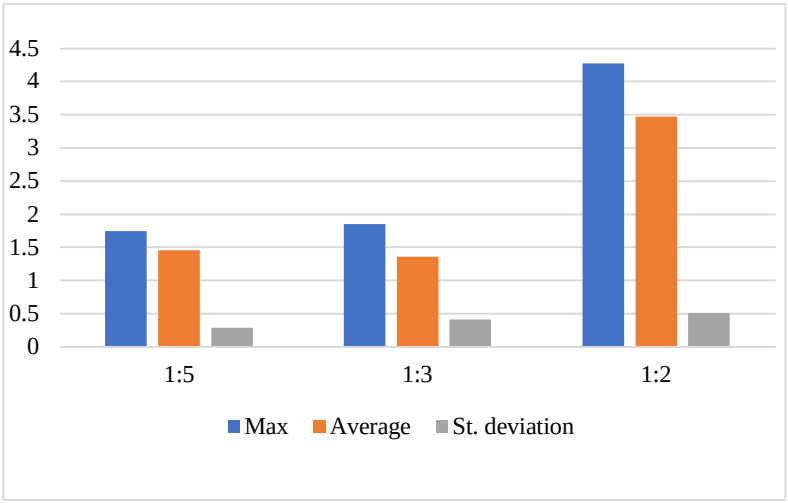

Fig. 2 The maximum, average, and standard deviation of the displacements of check points across different scenarios involving varying numbers of control points (*Experiment 1, r=1*)

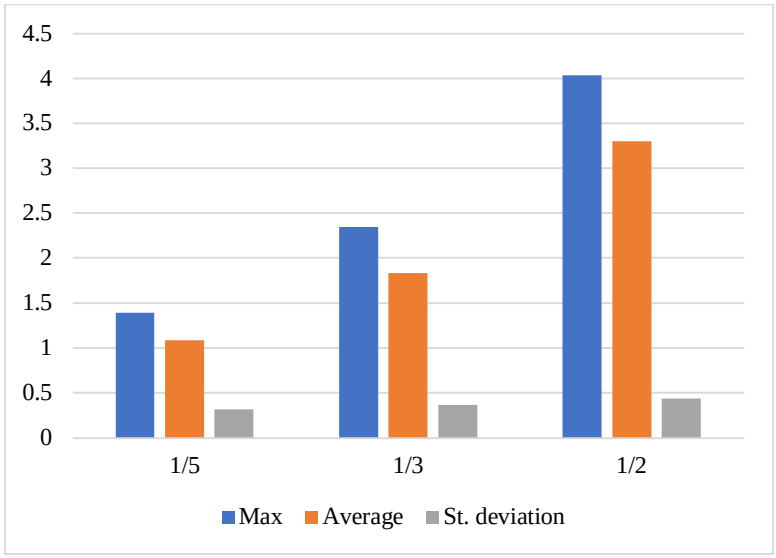

Fig. 3 The maximum, average, and standard deviation of the displacements of check points across different scenarios involving varying numbers of control points (*Experiment 1, r=2*)

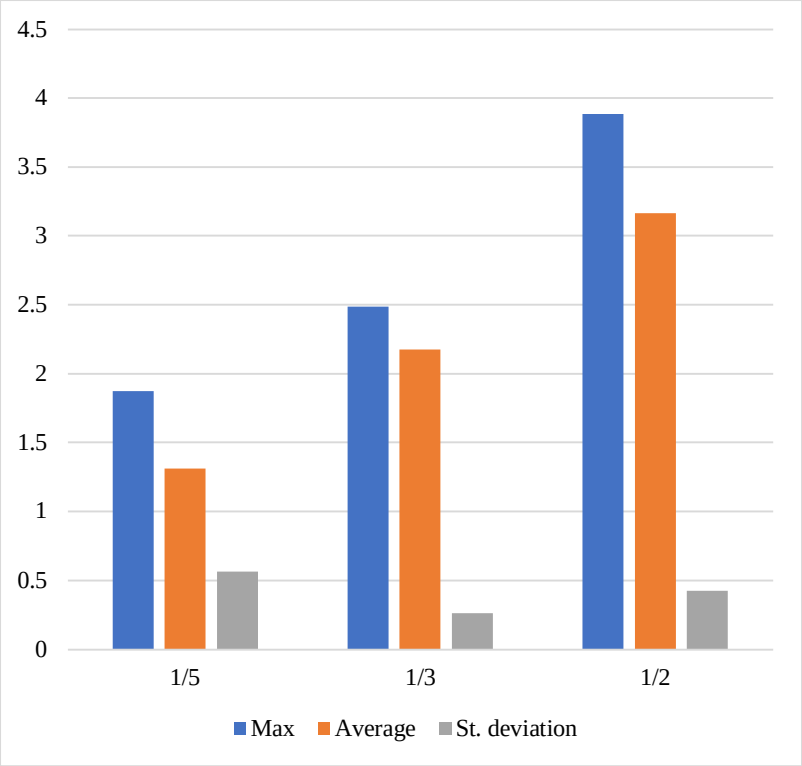

Fig. 4 The maximum, average, and standard deviation of the displacements of check points across different scenarios involving varying numbers of control points (*Experiment 1, r=3*)

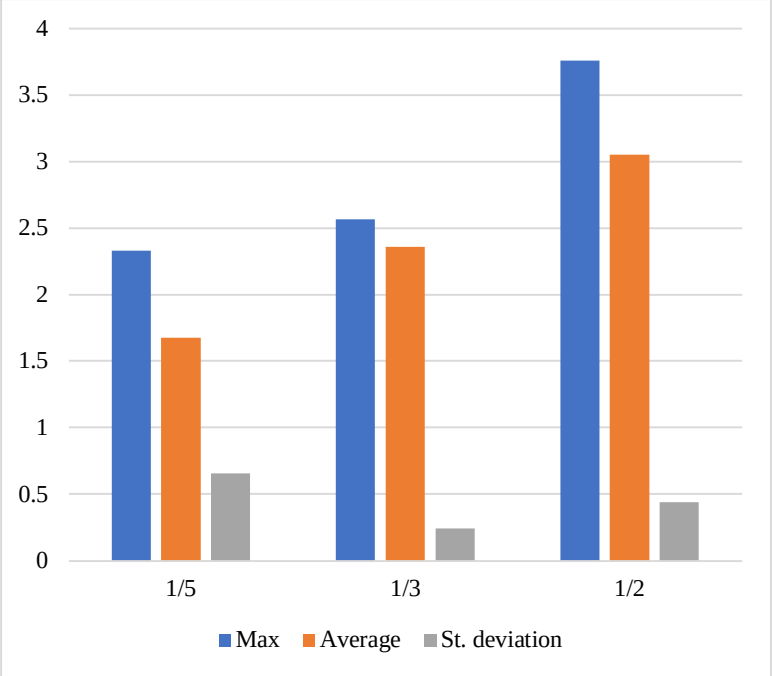

Fig. 5 The maximum, average, and standard deviation of the displacements of check points across different scenarios involving varying numbers of control points (*Experiment 1, r=4*)

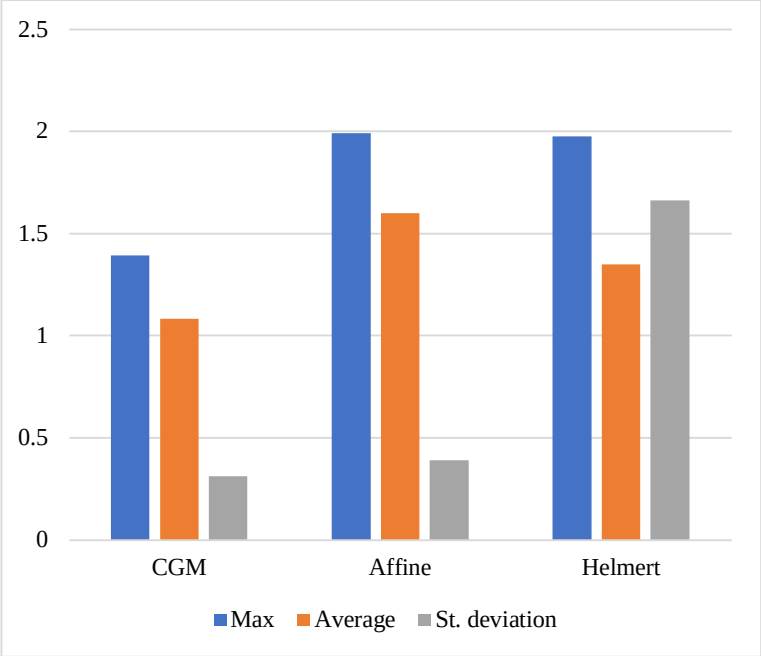

Fig. 6 The maximum, average, and standard deviation of the displacements of check points across different scenarios involving varying methods: CGM (*Experiment 1, r=2*), Helmert and Affine

Experiment 2: The CGM was applied using the cosine influence factor (as described in equation 3), tested with various values of *r* and different ratios of check points (Ch.P) to control points (CP), similar to the previous experiment. The figures show that using one check point with five control points produced better results. Figure 2 presents the maximum, mean, and standard deviation values of the displacements of check points from their actual positions after applying the Cosine Influence Factor with $r = 1$. The performance improved as *r* increased, but after $r = 5$, the results started to decline. Figures 7, 8, 9, 10, and 11 illustrate the outcomes for check points using the three specified ratios of Ch.P for *r* values ranging from 1 to 5. The experiment concluded that the second-degree linear Influence Factor provided the best results. Figure 6 compares the CGM (using the second-degree linear Influence Factor) with Affine and Helmert transformations, and Figure 12 further illustrates that the CGM outperformed both the Affine and Helmert methods.

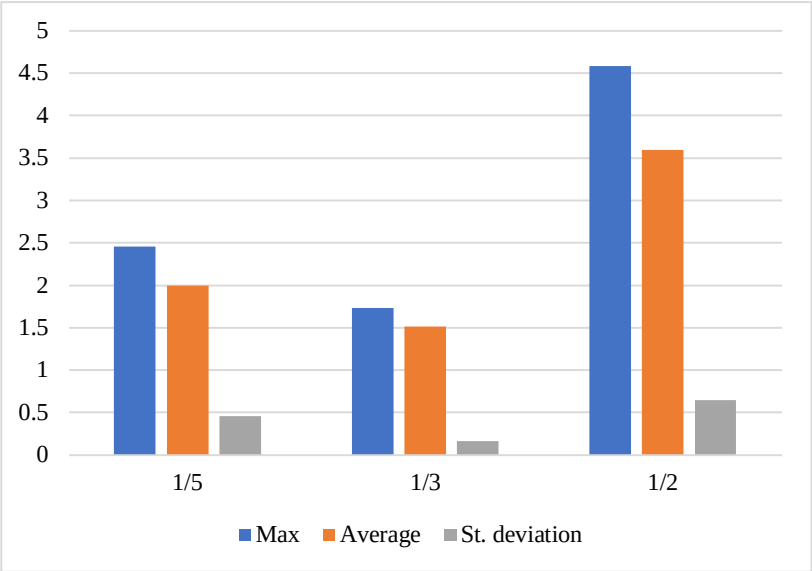

Fig. 7 The maximum, average, and standard deviation of the displacements of check points across different scenarios involving varying numbers of control points (*Experiment 2, r=1*)

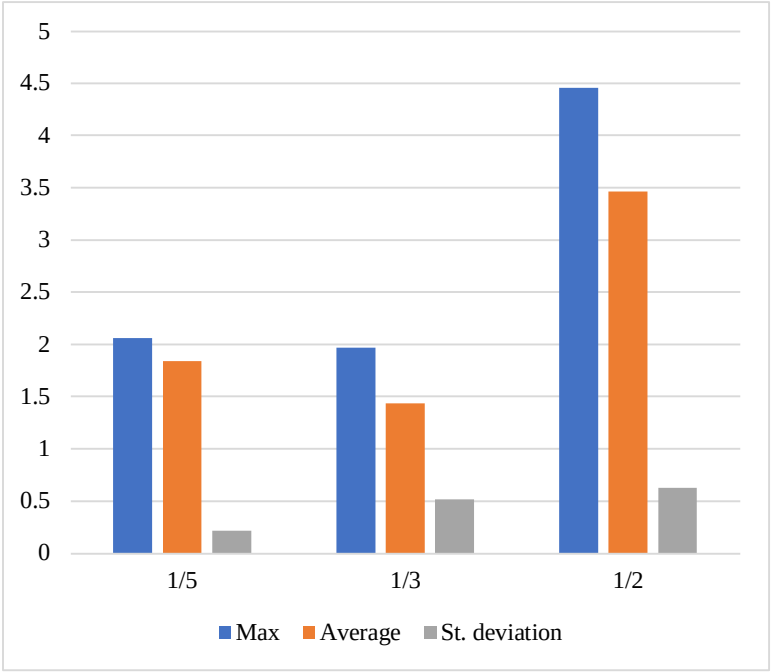

Fig. 8 The maximum, average, and standard deviation of the displacements of check points across different scenarios involving varying numbers of control points (*Experiment 2, r=2*)

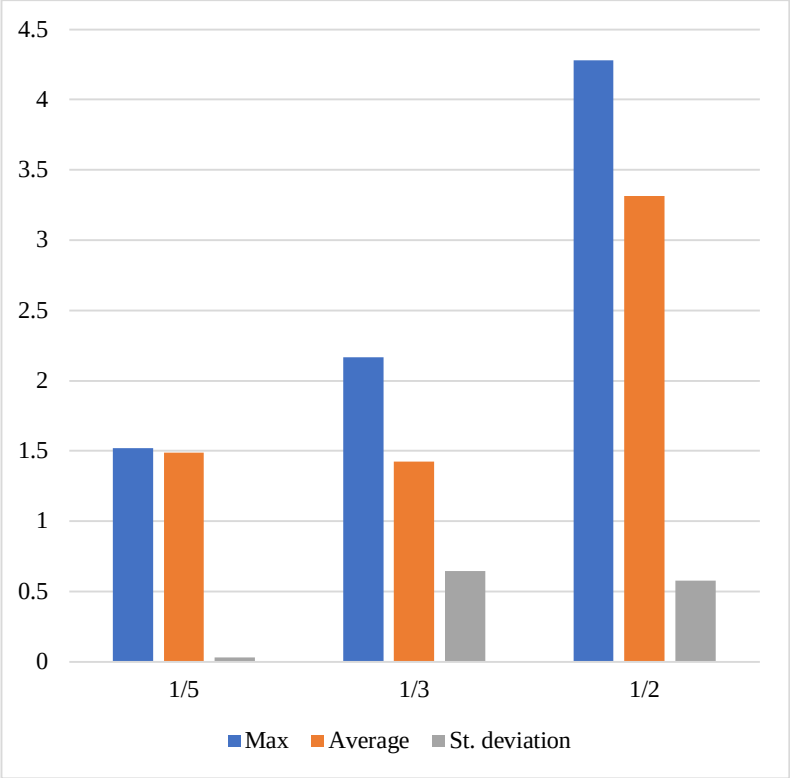

Fig. 9 The maximum, average, and standard deviation of the displacements of check points across different scenarios involving varying numbers of control points (*Experiment 2, r=3*)

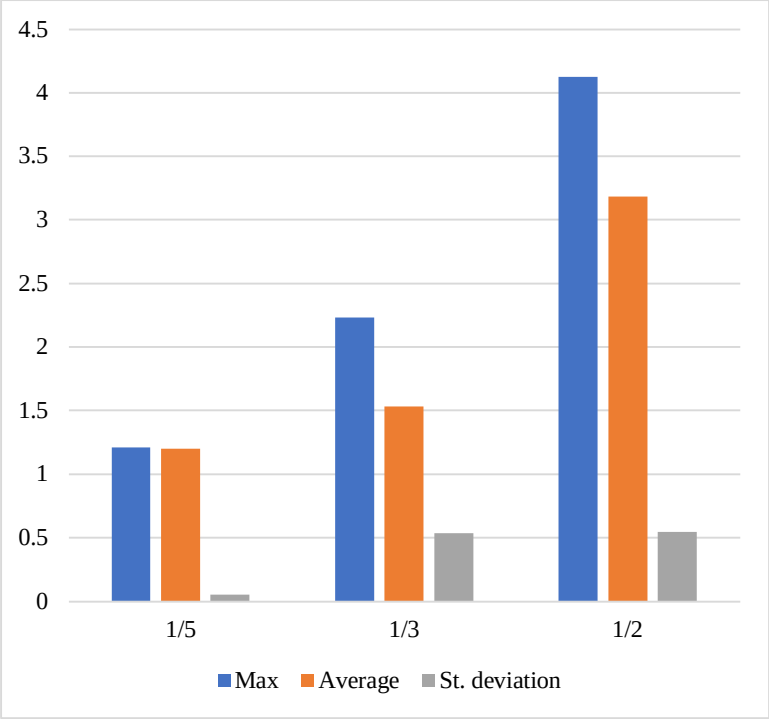

Fig. 10 The maximum, average, and standard deviation of the displacements of check points across different scenarios involving varying numbers of control points (*Experiment 2, r=4*)

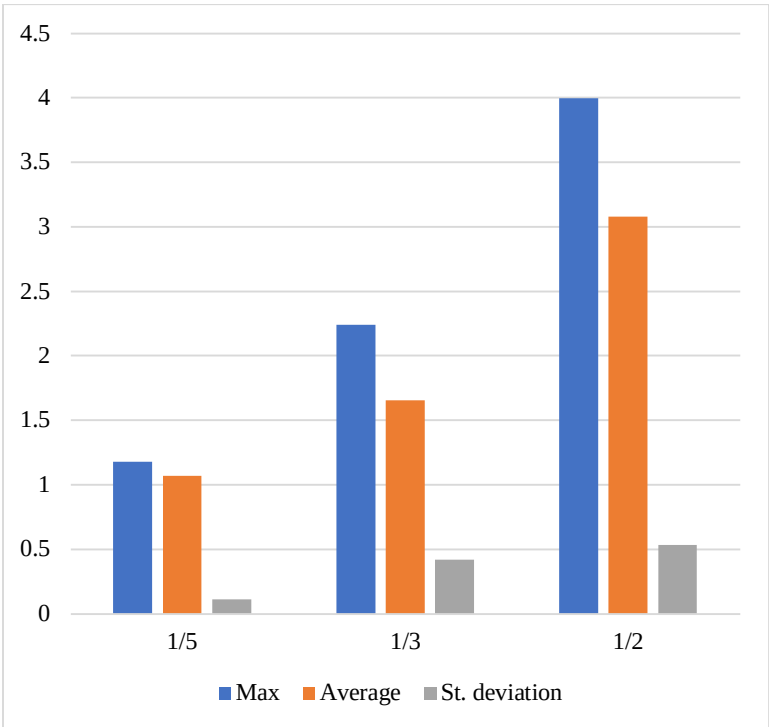

Fig. 11 The maximum, average, and standard deviation of the displacements of check points across different scenarios involving varying numbers of control points (*Experiment 2, r=5*)

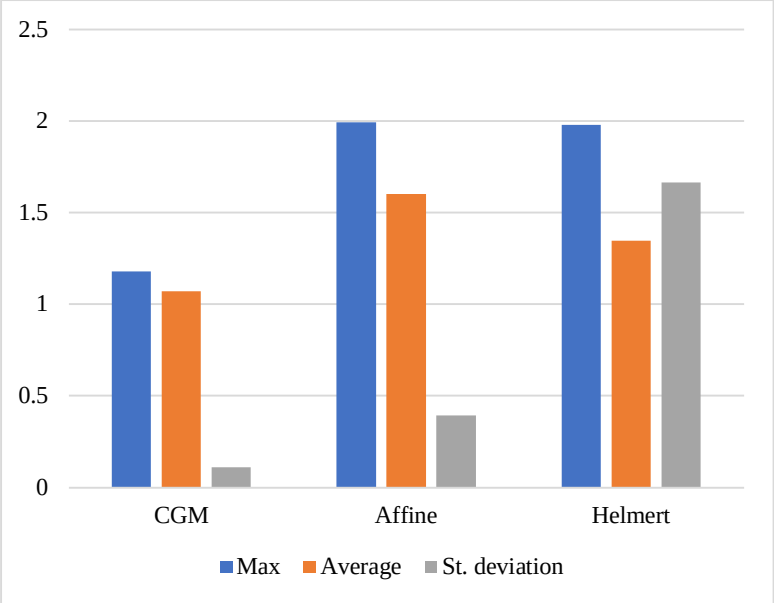

Fig. 12 The maximum, average, and standard deviation of the displacements of check points across different scenarios involving varying methods: CGM (*Experiment 2, r=5*), Helmert and Affine

Experiment 3 The CGM was applied using a linear Influence factor (as described in equation 4), with varying values of the internal parameter r and different ratios of check points (Ch.P) to modeling points: 1:5, 1:3, and 1:2, similar to the previous experiment. Here, as r increased, the results worsened, confirming that the first-degree tangent influence factor is the most effective. Figures 13, 14, 15, and 16 present the results for the check points under the three specified Ch.P ratios. After recalculating the new coordinates, the displacements of the check points from their actual positions were measured, and the maximum, average, and standard deviation of these displacements were determined. Figure 17 compares the performance of the CGM (using the first-degree tangent influence factor) with the Affine and Helmert transformations. The comparison shows that the CGM consistently delivers better results than both the Affine and Helmert methods.

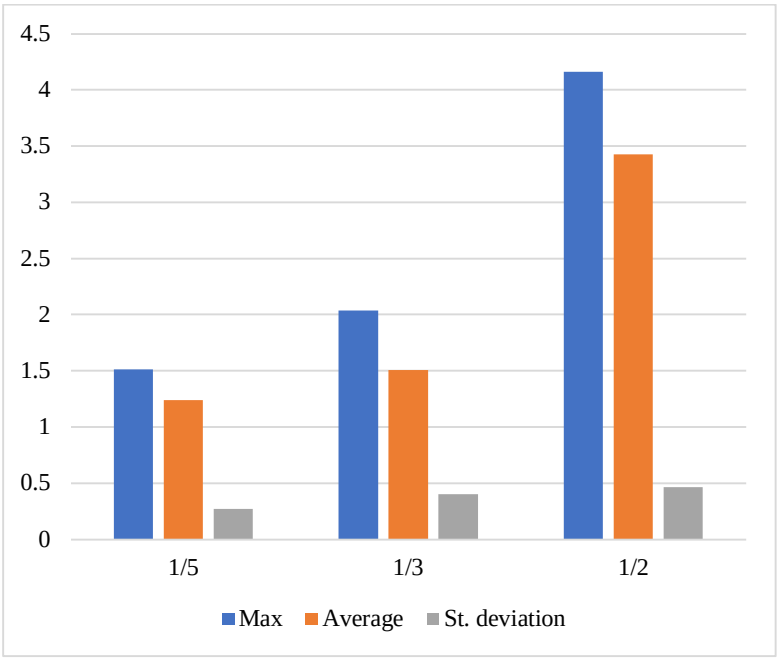

Fig. 13 The maximum, average, and standard deviation of the displacements of check points across different scenarios involving varying numbers of control points (*Experiment 3, r=1*)

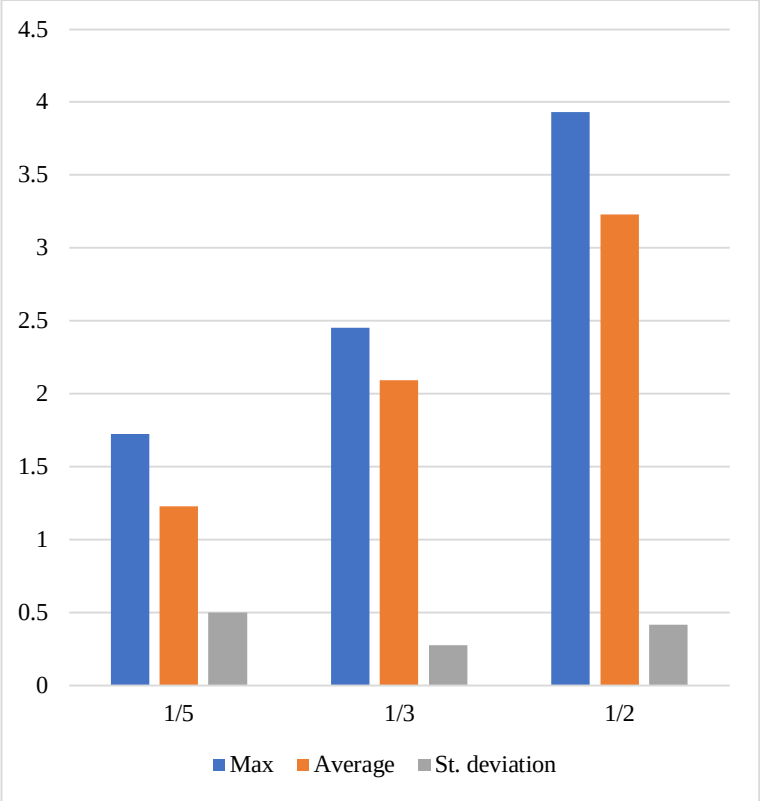

Fig. 14 The maximum, average, and standard deviation of the displacements of check points across different scenarios involving varying numbers of control points (*Experiment 3, r=2*)

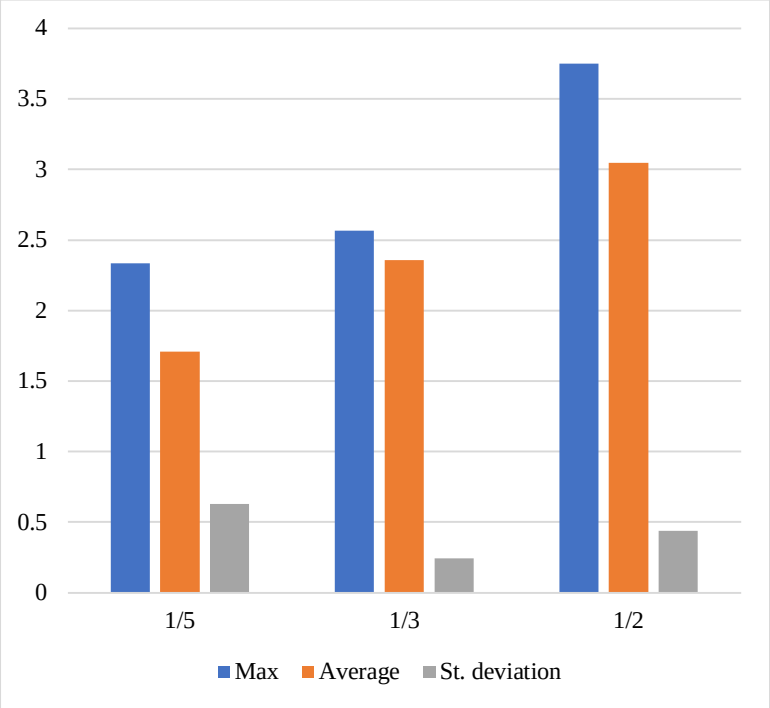

Fig. 15 The maximum, average, and standard deviation of the displacements of check points across different scenarios involving varying numbers of control points (*Experiment 3, r=3*)

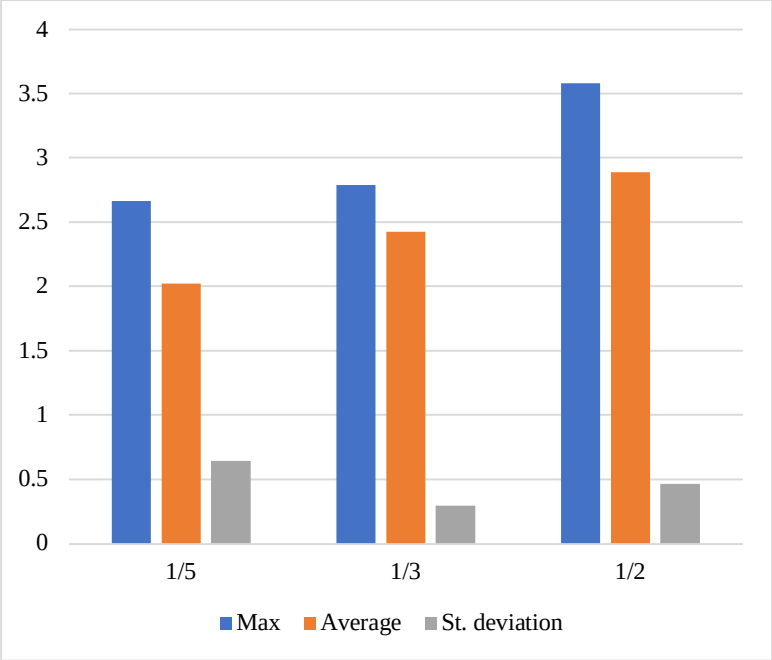

Fig. 16 The maximum, average, and standard deviation of the displacements of check points across different scenarios involving varying numbers of control points (*Experiment 3, r=4*)

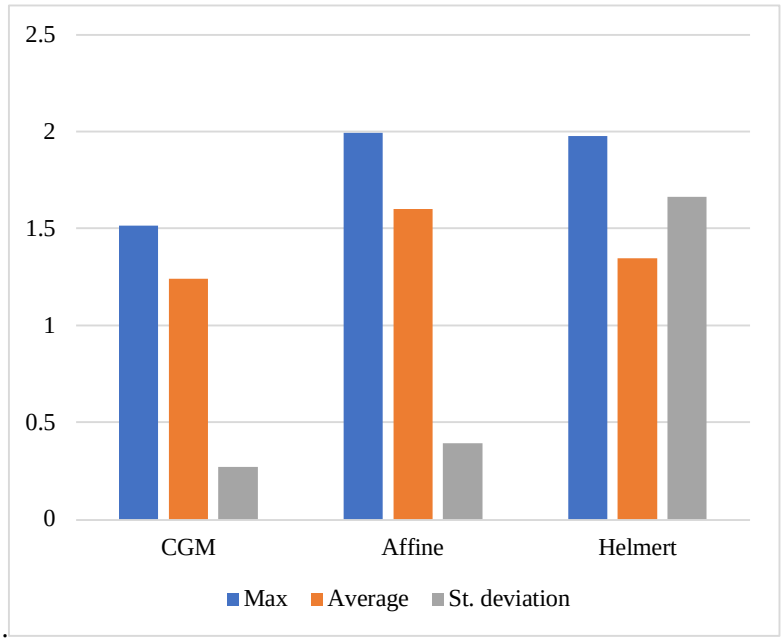

Fig. 17 The maximum, average, and standard deviation of the displacements of check points across different scenarios involving varying methods: CGM (*Experiment 3, r=1*), Helmert and Affine

V. CONCLUSION

Figure 18 presents a summary of the final results, showing that all experiments yield better outcomes compared to the traditional Helmert and Affine methods. Notably, it demonstrates that the fifth-degree Cosine Influence Factor is the optimal choice for applying CGM. In Figure 19, it is shown that for about the first quarter of the maximum distance in the image, the cosine and Tangent Influence Factors behave similarly, whereas the linear Influence Factor has a weaker effect.

Beyond this point, the linear and Tangent Influence Factors decrease at the same rate, while the Cosine Influence Factor steepens, indicating a more rapid decline in its effect. This faster reduction seems to contribute to the improved performance. In the final quarter of the maximum distance, the Cosine Influence Factor flattens, becoming nearly horizontal. This suggests that beyond three-quarters of the maximum distance, the displacement of a point has minimal or no effect on other points in the image.

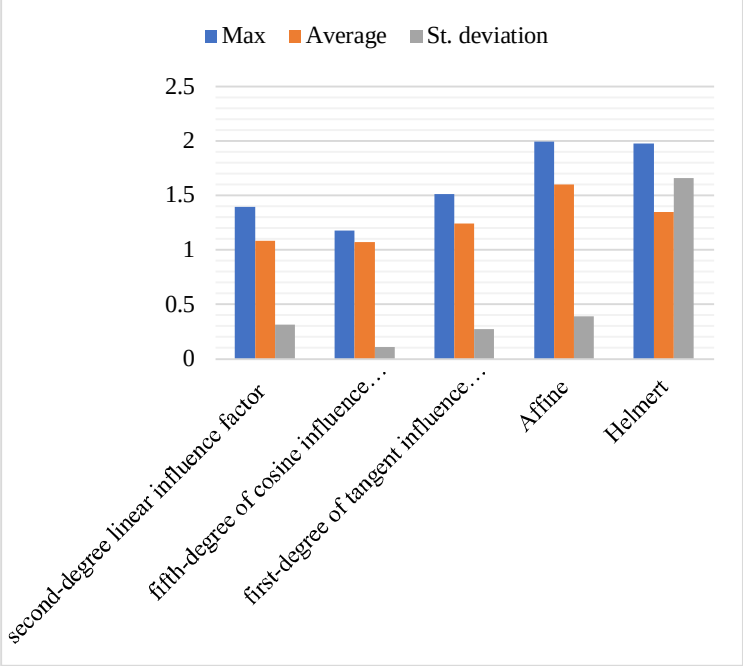

Fig. 18 The results of the CGM, using the optimal value of r, are compared with the Affine and Helmert transformation methods.

Figure 19 illustrates that, for approximately the first quarter of the maximum distance in the image, the Cosine and Tangent Influence Factors behave similarly, while the linear Influence Factor has a weaker effect. Beyond this range, the linear and Tangent Influence Factors exhibit the same rate of decrease, while the curve of the Cosine Influence Factor becomes steeper than the others, indicating a faster reduction in its effect. This rapid decrease may contribute to the improved results observed. In the last quarter of the maximum distance, the Cosine Influence Factor levels off, becoming nearly horizontal. This suggests that displacing a point has little to no Influence on other points that are more than three-quarters of the maximum distance apart in the image.

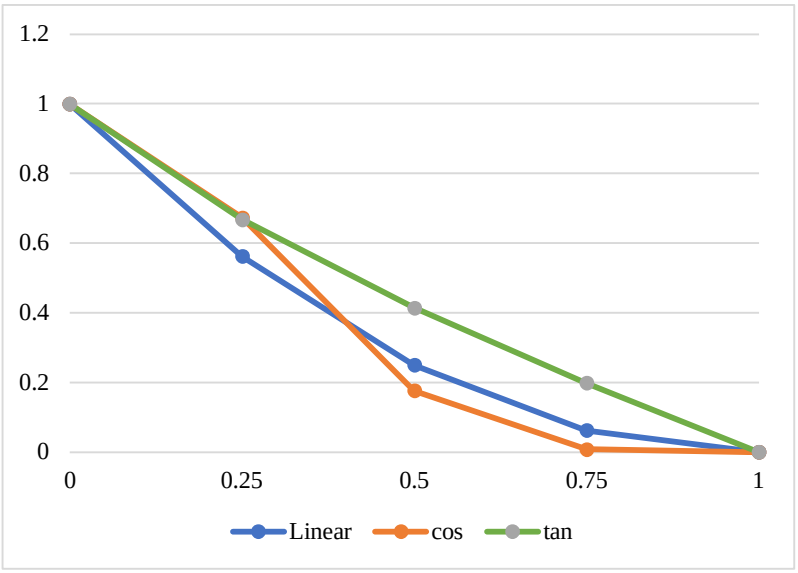

Fig. 19 An illustration of the behavior of the three proposed Influence factors—Linear, Cosine, and Tangent

VI. COMPETING INTERESTS

No funding was received for conducting this study. There is no conflict of interest.

REFERENCES

[1] Angela M. Peters and Robert J. Smith, 2022. "The Use of Control Points in Image Georeferencing: A Critical Review"
[2] Chiabrando, F., Donadio, E., & Rinaudo, F, 2016. "Automated Georeferencing of Historical Maps Using Machine Learning and Crowdsourcing Techniques", ISPRS International Journal of Geo-Information.
[3] Ian H. Campbell and Naomi L. Wilke, 2020. "Automated Image Georeferencing Using OpenStreetMap Data"
[4] Jennifer L. McDaid and David W. Long, 2019. "A Comparative Study of Georeferencing Algorithms for Historical Maps"
[5] Johnson, M., & Wang, Y, 2019. "Performance Comparison of Automated and Manual Georeferencing Methods for High-Resolution Satellite Images"
[6] Lee, H., & Park, S., 2021. "A Comparative Study of Georeferencing Algorithms Using OpenStreetMap Data"
[7] Li, D., Wang, J., & Zhang, X., 2012. "Georeferencing of Satellite Images Using Ground Control Points and Feature Matching Techniques", Photogrammetric Engineering & Remote Sensing.
[8] Liu, X., & Chen, G., 2020. "Hybrid Georeferencing Approaches: A Comparative Study"
[9] Liu, X., Zhang, Y., & Chen, G., 2018. "Hybrid Georeferencing Method for High-Resolution Satellite Imagery"
[10] Maria B. Johnson and Kevin R. O'Reilly, 2021. "Georeferencing of Remote Sensing Images with Convolutional Neural Networks"
[11] Martinez, J., & Garcia, L., 2017. "Comparison of Georeferencing Methods for Historical Map Rectification"
[12] Rumsey, D., & Williams, M., 2002. "Georeferencing Historical Maps in a GIS Environment", Cartography and Geographic Information Science.
[13] Smith, R., & Brown, T., 2018. "Evaluating the Accuracy of Image Georeferencing Techniques in Remote Sensing"
[14] Yuan, F., & Elaksher, A., 2007. "Georeferencing of Historical Aerial Photographs Using GIS and Image Processing Techniques", IEEE Geoscience and Remote Sensing Letters.
[15] Zhang, L., & Luo, H., 2018. "Real-time Image Georeferencing Using UAV-Based Remote Sensing", Remote Sensing.

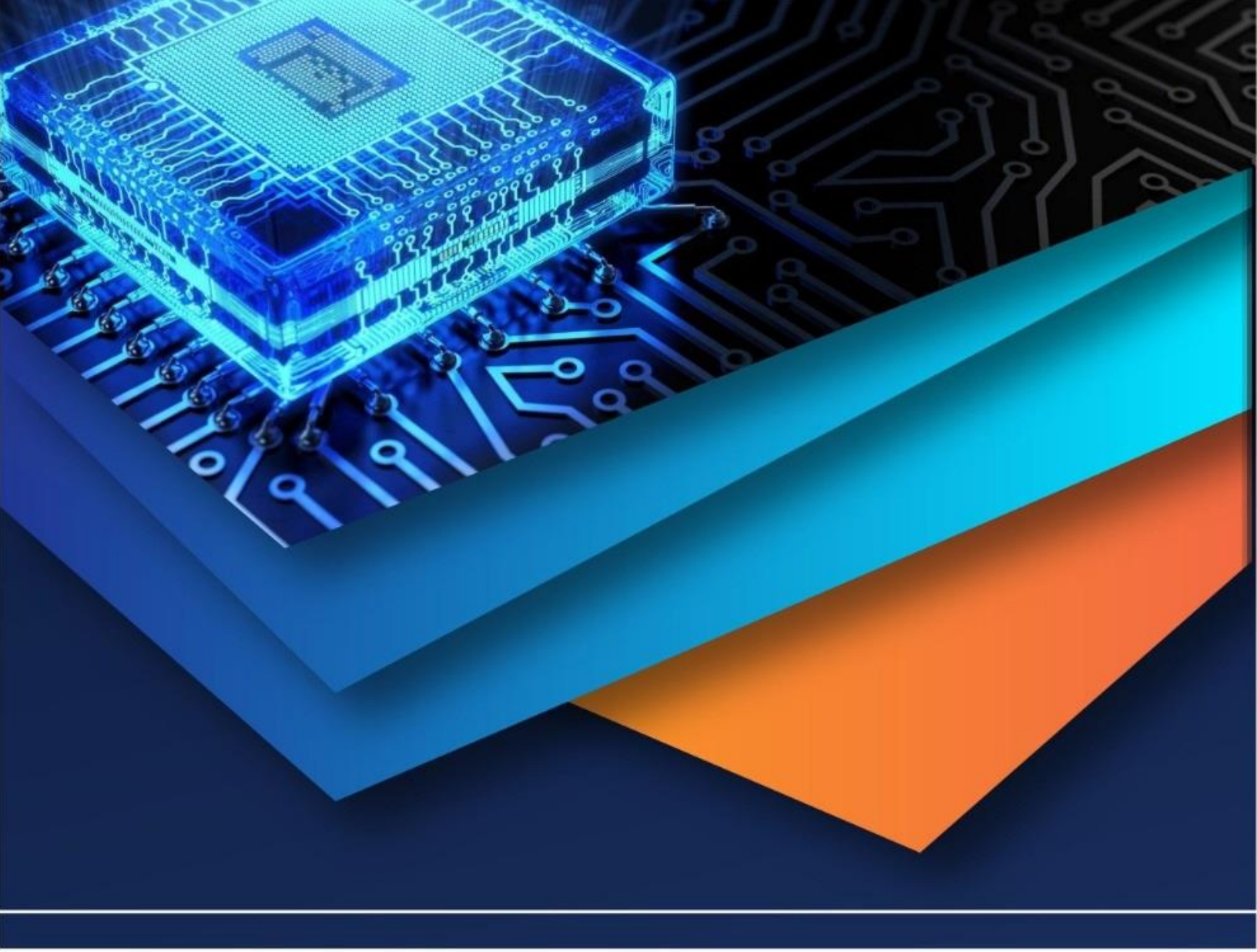

10.22214/IJRASET

45.98

IMPACT FACTOR: 7.129

IMPACT FACTOR: 7.429

INTERNATIONAL JOURNAL FOR RESEARCH

IN APPLIED SCIENCE & ENGINEERING TECHNOLOGY